

Photonic-Crystal Scintillators: Molding the Flow of Light to Enhance X-Ray and γ -Ray Detection

Yaniv Kurman¹, Avner Shultzman¹, Ohad Segal¹, Adi Pick², and Ido Kaminer^{1,*}

¹*Department of Electrical Engineering, Technion, Israel Institute of Technology, 32000 Haifa, Israel*

²*Department of Chemical Physics, Weizmann Institute of Science, Rehovot 76100, Israel*



(Received 16 February 2020; accepted 23 June 2020; published 22 July 2020)

Scintillators are central for detection of γ -ray, x-ray, and high energy particles in various applications, all seeking higher scintillation yield and rate. However, these are limited by the intrinsic isotropy of spontaneous emission of the scintillation light and its inefficient outcoupling. We propose a new design methodology for scintillators that exploits the Purcell effect to enhance their light emission. As examples, we show 1D photonic crystals from scintillator materials that achieve directional emission and fivefold enhancement in the number of detectable photons per excitation.

DOI: [10.1103/PhysRevLett.125.040801](https://doi.org/10.1103/PhysRevLett.125.040801)

Detection of energetic particles is most commonly achieved by using the scintillation process. The scintillation process lies at the heart of a wide range of technologies, from medical tomography systems such as positron emission tomography (PET) and computed tomography (CT) [1,2], to industrial uses such as light intensifiers and security scanners, and even scientific facilities such as electron microscopes and particle accelerators [3]. Through a chain of processes, a scintillator converts the incoming radiation's energy into visible light, which is then detected with various photodetection capabilities [4]. The energy is converted in scintillators in the following manner: the energetic radiation produces a single photoelectric electron or one or more Compton electrons, which then excite many electron-hole pairs that thermalize until reaching luminescence centers, where each pair can recombine radiatively by emitting spontaneous emission, which is the desired signal that we detect.

Recent works have reported several types of novel approaches to improve scintillation timing and efficiency. The approaches include changing the scintillator macroscopic dimensions [5–7], improving the read-out electronics [8], developing new scintillation materials [9–11], and embedding fast emitting materials inside bulk scintillators [12,13]. Another pathway that drew much attention involves refining the light extraction of the scintillator emission using photonic crystals as impedance matching layers between the scintillator and the photodetector [14–21]. However, in all works so far, the actual emission from the scintillator has always been considered an intrinsic property of the material [22–24].

In this Letter, we show how the design of artificial nanophotonic structures made from combinations of intrinsic scintillators with other dielectric materials can improve the scintillation efficiency and timing compared to a bulk scintillator. In order to modify and enhance intrinsic

emission properties, the entire structure is designed with features on length scales comparable to the scintillation emission wavelength (hundreds of nanometers). Our approach differs from the previous usages of nanophotonics to manipulate the already-created scintillation emission [8]. Instead, we enhance the intrinsic emission process of the scintillator by exploiting the Purcell effect. This way, we enhance the scintillator's emission into detectable directions, while inhibiting the undetectable scintillator emission. As a result, a photonic designed scintillator reduces dramatically the number undetectable, total internal reflected, photons of the conventional isotropically emitting bulk scintillators. We show a factor of 5 enhancement in outcoupling efficiency for a one-dimensional (1D) photonic crystal (PhC) structure, i.e., a medium made from periodically alternating layers, made from scintillator materials [shown in Fig. 1(a)]. Our work also develops a framework that analytically analyzes the scintillator characteristics in a general optical structure. We demonstrate the framework by using the properties of standard scintillation materials, LYSO:Ce [25] and Gd₂O₂S:Tb [26]. Consequently, one can enhance the sensitivity and timing of a scintillator or produce the same signal with less radiation exposure or with lower amounts of scintillation material.

The control over the emission process of an emitter by the Purcell effect has been shown in many atomic and molecular systems over the years [27–32], but has never been used in scintillators. According to the Purcell effect, the design of an optical structure around a pointlike, dipole, emitter can change the density of photonic states to enhance or suppress emission in specific directions and frequency ranges by the Purcell factor F_p . In such cases, the design rule of thumb is to increase the quality factor Q and to reduce the photonic mode volume V at the frequency of the emitter, since $F_p \propto Q/V$. However, these design rules are exactly the *opposite* of what is needed for a scintillation

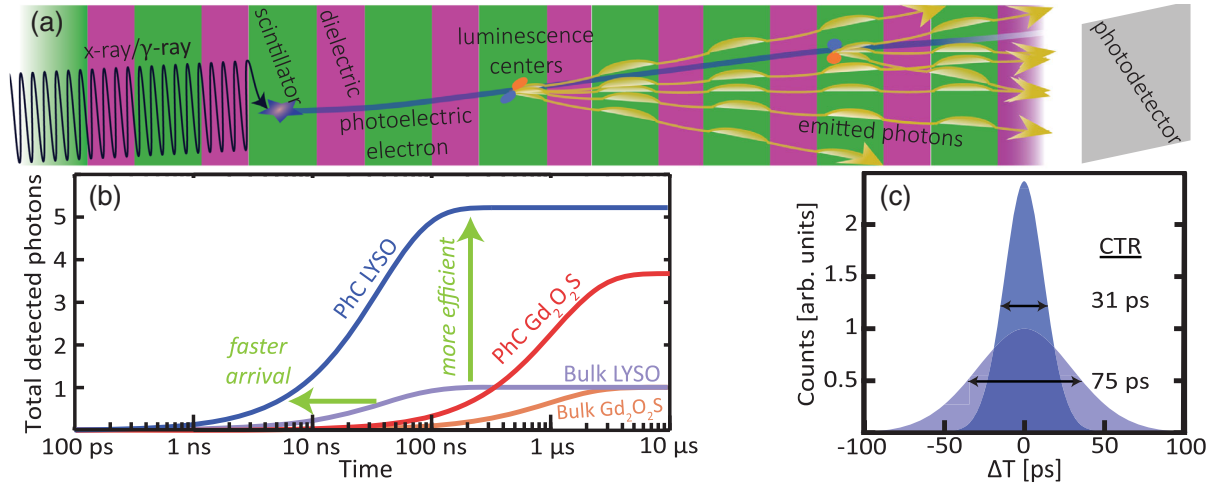


FIG. 1. Photonic crystal scintillator: illustration and main results. (a) Illustration of the scintillation process. An incident energetic photon (x ray or γ ray) is converted by the scintillator material (green) into an energetic electron (e.g., photoelectric electron, blue), which excites a large number of electron-hole pairs. The electron-hole pairs thermalize until reaching luminescence centers and radiatively recombine while emitting light only into the possible photonic modes of the structure (yellow). The PhC is designed so that most of these modes are coupled out and detected by a photodetector (e.g., silicon photomultiplier, gray). By alternating wavelength-size layers of a scintillator material (green) and another dielectric material (pink), the photonic modes can be shaped, and the emission process can be controlled. (b) The number of detectable photons over time, normalized to the total number of detectable photons for a bulk scintillator with the same scintillation volume. We present the results of a LYSO:Ce/air PhC with the emission coupled out to air (blue curves), and of a Gd₂O₃S:Tb/SiO₂ PhC with the emission coupled out to SiO₂ (red curves). The PhC structure enables more detectable photons with a faster emission rate. (c) The coincidence time resolution (CTR) that correlates two detectors, measuring the arrival times of the first (detected) photon in each detector. The CTR determines the resolution for PET scans and other time-of-flight applications. The PhC structure enhances the CTR by a factor of 2.4.

structure, since the luminescence centers span the entire scintillator volume, and a low Q is required for an efficient outcoupling. Thus, the design of the scintillation structure must follow a completely different rule of thumb: The scintillation structure should support extended optical modes that outcouple efficiently to the surrounding optical environment (low Q and large V), while still being emitted at a high rate.

Photonic crystal structures can enhance both the efficiency η and the effective emission rates Γ_{eff} (defined below) of the scintillation process. The periodicity of the refractive index causes the modes of light to form photonic Bloch modes, with a dispersion relation that constructs a photonic band structure (analogous to the electronic band structure in solids). Varying the width of each layer modifies the photonic band structure and thus control the photonic local density of states (LDOS) for each frequency and propagation angle (as well as polarization). We utilize the analytical formulas of a 1D PhCs using the dyadic Green's function to find the required widths of the layers that optimize a specific figure of merit [33]. As an example, we maximize the multiplication between the efficiency and the emission rate of the detectable photons. In Fig. 1(b), we show the number of detectable photons over time, calculated as a cumulative distribution function times the efficiency η (see Supplemental Material [33], Sec. S.2). The right edge of the plot (long time) shows that the efficiency can be enhanced by a factor of above 5,

which also improves the scintillation sensitivity and the energy resolution.

The figure of merit used in the example in Fig. 1 is particularly useful for applications in which both the time resolution and efficiency are important, such as time-of-flight PET and other time-of-flight detection in particle accelerators [24,36,37]. In these applications, the spatial resolution is determined by the variance of the first photon arrival time, called the coincidence time resolution (CTR), found by the short-time signal in Fig. 1(b). Combining our theory with the conventional statistical model of ultrafast light detection [36,38], we find a convenient formula for the CTR reduction, $\text{CTR}_0/\text{CTR} = \sqrt{\eta\Gamma_{\text{eff}}\tau_{d,0}}$, where CTR_0 and $\tau_{d,0}$ are the CTR and decay time in a bulk scintillator respectively. We find that an optimized PhC structure reduces the CTR by a factor of 2.4, promising a major resolution improvement in any time-of-flight application [39].

Our theoretical analysis requires two useful definitions, the Purcell factor $F_P^\sigma(\mathbf{r}, \omega, \theta)$ and the transmission coefficient $T^\sigma(\mathbf{r}, \omega, \theta)$; both definitions depend on the location in space \mathbf{r} , the frequency ω , the emission angle θ relative to the normal to the layers (z), and the polarizability σ . The Purcell factor relates to the emission rate enhancement comparing to the emission rate in vacuum. The goal of maximal efficiency requires considering the outcoupling of each mode, which is captured by combining the Purcell

factor with the transmission coefficient. We define the effective emission rate Γ_{eff} as the number of photons per unit time that arrive at the detector outside the scintillator material:

$$\Gamma_{\text{eff}} = \int d\omega Y(\omega) \int_0^{\pi/2} \sin(\theta) d\theta \times \int_0^L dz G(z) \sum_{\sigma} \Gamma_0^{\sigma}(\omega) F_p^{\sigma}(z, \omega, \theta) T^{\sigma}(z, \omega, \theta), \quad (1)$$

where L is the finite structure length, and $\Gamma_0^{\sigma}(\omega)$ is the emission rate in vacuum for a specific polarization and frequency. $G(z)$ and $Y(\omega)$ are the spatial and frequency distribution of the emitters, respectively [normalized by $\int G(z) dz = 1$ and $\int Y(\omega) d\omega = 1$]. $Y(\omega)$ can be understood as the amount of luminescence centers with emission frequency ω compared to the total amount of luminescence centers. Accordingly, the decay time of the scintillator is in fact $\tau_d = 1/\Gamma_{\text{eff}}$. We can similarly define the decay time in bulk as $\tau_{d,0} = 1/\Gamma_{\text{eff},0}$, using a similar calculation to Eq. (1) but in a bulk material. Details are in the Supplemental Material [33], Sec. II.

As opposed to the effective emission rate, which is important for timing applications, many radiation detection applications try to maximize the number of detectable photons per excitation. The efficiency η is defined as

$$\eta = \frac{\text{\# of detectable photons in the PhC}}{\text{\# of detectable photons in the bulk}} = \frac{\Gamma_{\text{eff}}}{\Gamma_{\text{tot}}}, \quad (2)$$

where Γ_{tot} and $\Gamma_{\text{tot},0}$ are the total emission rates in the PhC and in the bulk, respectively. Importantly, the entire

dependence on the exact geometry of the structure in Eqs. (1) and (2) is through F_p^{σ} and T^{σ} . Therefore, the same theory holds for predicting the scintillation rate and efficiency in any general geometry.

In the specific case of a 1D PhC structure, we have determined the layer width of each material to maximize $\eta\Gamma_{\text{eff}}$ using an interior-point optimization algorithm [40], while fixing the environment and each material's refractive index. In table S1 [33], we show the parameters for the optimized LYSO:Ce/air PhC and Gd₂O₂S:Tb/SiO₂ PhC that were used for each plot in the Letter. These materials were chosen as examples since they are the leading scintillation materials in radiology and CT scans (doped Gd₂O₂S) [41] and in nuclear imaging machines such as PET scans (doped LYSO) [36]. In the Supplemental Material [33] Secs. S.4 and S.5 we show how to derive analytically the Purcell factor and transmission coefficient for any 1D layered structure (finite or infinite), with the required input being only the refractive index of each material. Numerical tests show that these coefficients gradually become independent of the number of layers for thicker structures.

In order to investigate the underlying mechanism by which a PhC enhances scintillation, we present in Fig. 2(a) the emission rate enhancement for each wavelength and in-plane momentum (k_x). The emission rate is calculated by averaging over the locations and random polarization of the luminescence centers in the entire structure. Figure 2 reveals the importance of the PhC band structure for the design of PhC scintillators. For each emission wavelength, the photonic band structure shows emission enhancement to some angles and emission reduction into other angles. By optimizing the structure, we match the enhanced angles

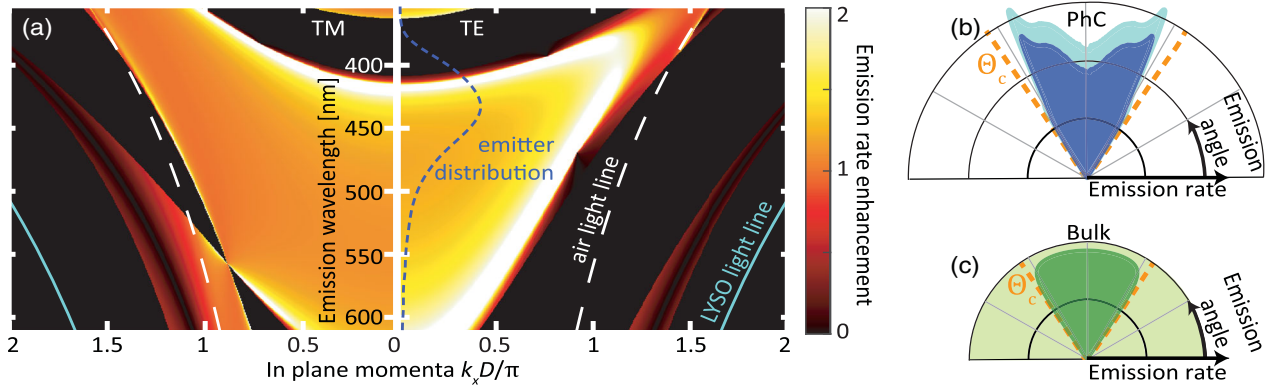


FIG. 2. The photonic-crystal scintillator emission features. (a) The emission rate enhancement for each in-plane momentum k_x and wavelength, calculated for an infinite LYSO/air PhC with period D . The geometrical features of the structure are optimized to fit the emitter spectral distribution (dashed blue). (b) The total emission rate for the PhC (turquoise) and the outcoupled part (blue) as a function of emission angle, normalized by the bulk emission rate. In the PhC structure, the emission is created below the critical angle θ_c (orange), and thus the efficiency is enhanced. (c) The total emission rate for the bulk (light green) and the outcoupled part (green) as a function of emission angle. The emission into angles beyond the critical angle (orange) is undetectable. The PhC effective emission rate enhancement is the ratio between the blue area in (b) and the green area in (c). The luminescence centers are assumed homogeneous and with random dipole orientation. The analytical expressions for these plots are derived in the Supplemental Material [33], Sec. S.6.

to ones that efficiently outcouple, and the inhibited angles to ones that do not outcouple. That is, we design the PhC so that the LDOS of the detectable modes is increased, while the LDOS of the undetectable modes is minimized (e.g., compare the map above versus below the air light line, white dashed). Figure 2(a) also shows how an optimized photonic structure imposes the largest emission rate enhancement exactly at the peak of the emitter’s spectral distribution $Y(\omega)$ (dashed blue). This plot assumes a thick PhC such that the edges can be neglected. We find in Fig. S2 of the Supplemental Material [33] that similar features are formed after just a few periods (e.g., the photonic band gap appears after three periods).

More generally, the PhC materials and dimensions can be chosen to fit every emission spectral distribution by “stretching” and “shifting” the same typical photonic band structure [42]. As a rule of thumb, a larger refractive index contrast between the two materials in the PhC increases the potential advantages from the PhC properties. Interestingly, the control over the emission angles is possible even in unintuitive cases such as when the scintillator material has a lower refractive index than the other material(s) used to create the PhC. If the surrounding material has a larger refractive index (for example a silicon chip detector), the original outcoupling efficiency is larger and the PhC should be optimized for other parameters such as the emission rate or the directionality of emission.

In Figs. 2(b) and 2(c) we see how the PhC band structure in our LYSO:air example translates into enhancing Γ_{eff} and η . Figure 2(b) presents the emission rate enhancement per emission angle, obtained once multiplying the result in Fig. 2(a) by the spectral distribution (dashed blue) and integrating over frequency. We find that inside the PhC structure (turquoise), only light that propagates below the critical angle is created. Compared to the emission features in a bulk structure [Fig. 2(c)], the efficiency of the entire scintillation process is enhanced by a factor of 5, shown by comparing the detectable photons (green and blue) to the total emission (light green and turquoise). Moreover, the larger rate of detectable photons relate to more outcoupled photons per second and lead to a 15% larger effective emission rate (blue compared to green).

The concept of a Purcell-enhanced scintillator can be extended in various ways. Instead of randomly oriented dipoles, a control over the dipole orientation of the luminescence centers can significantly improve the scintillation. Such a control can be achieved, for example, by using perovskite platelets with emitters in which the dipole moments are all aligned [43]. We show in Fig. 3(a) that even without further optimization of the PhC in Fig. 2, the emission rate $\Gamma_{\text{eff}}\tau_{d,0}$ can increase by almost a factor of 2 for an in-plane oriented dipole, so that $\eta\Gamma_{\text{eff}}\tau_{d,0}$ is increased by more than a factor of 8. Additional ways of improving the Purcell-enhanced scintillator are using scintillator materials with a narrower spectrum $Y(\omega)$, for which our

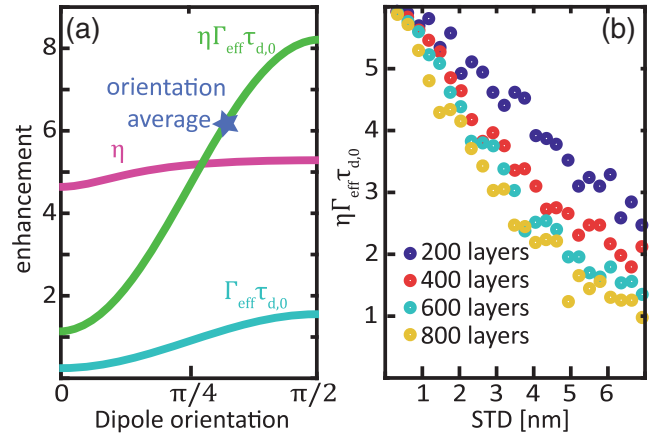


FIG. 3. Control and robustness of the photonic-crystal scintillators. (a) Enhancing scintillation by controlling the dipole orientation of the luminescence centers. The plot shows the efficiency η , and effective emission rate Γ_{eff} normalized by $\tau_{d,0}$ as a function of the dipole orientation relative to the z axis for the structure from Fig. 2. When the dipoles are oriented in the in-plane direction (angle $\pi/2$) the effective emission rate is enhanced, leading to an overall enhancement factor of above 8. (b) The overall enhancement of $\eta\Gamma_{\text{eff}}\tau_{d,0}$ as a function of the standard deviation (STD) of each LYSO layer width, for a different number of layers. As the randomness increases, Anderson localization reduces the transmission of light, and the overall response decreases.

figure of merit $\eta\Gamma_{\text{eff}}\tau_{d,0}$ is enhanced from 5.8 to above 6.5 (Fig. S5 [33]) without any additional structural change. We expect optimized PhC designs for a narrower emission spectrum to enable far better performances.

Other improvements of the Purcell-enhanced scintillator concept include designs of 2D and 3D PhC, or even more complex structures that can be created using 3D printers. Further optimization schemes could help reach ultimate scintillator performances in emission rates, which are theoretically bounded only by the emission frequency bandwidth [44]. Noticeably, the PhC structure can also improve additional channels that convert radiation to light, such as the fast photon emission of Cherenkov radiation [45]. In typical bulk materials, Cherenkov radiation is emitted when an energetic particle moves faster than the speed of light in the material, however in PhC structures this condition is modified significantly and can provide additional ways to enhance the Cherenkov signal [46].

It is imperative to consider the feasibility of fabricating PhCs from scintillation materials. Production of thin-film plastic scintillators [47] and thin-film inorganic scintillators [48] has been shown before. However, for some applications multiple layers must be created, for example, up to 10 000 layers (each being submicron in thickness) to stop γ rays. We show in Fig. 3(b) the fabrication tolerance needed to keep the photonic crystal properties. When increasing the standard deviation (STD) of each layer thickness,

optical Anderson localization [49] becomes an important factor in the design, so that the transmission of light and its outcoupling efficiency decrease. Moreover, when increasing the number of layers, the allowed STD reduces. Nevertheless, such accurate designs have been achieved in optical components (e.g., accurate band-pass filters) using several thin-film growth methods [50], and applied for various applications such as angular selective filters [51]. Other methods have shown consistent thicknesses over hundreds (and even thousands) of layers using polymer-stretching techniques (e.g., Ref. [52]). These nanofabrication techniques, combined with additional micromachining techniques (as chemical etching), would have to be used with scintillator materials or dopants to form the scintillator nanostructures.

Because of fabrication challenges, we expect the first applications of PhC scintillators to be ones where a smaller radiation stopping length is sufficient, thus requiring a smaller number of layers (roughly, tens of layers to stop keV electrons and hundreds of layers to stop soft x ray). Such applications include light intensifiers, electron cameras, and projectional radiography machines [53], in which the scintillators detect electrons or lower x-ray energies. In each application, whether medical or industrial, the scintillator geometry could be optimized using our method to a different figure of merit (e.g., see Supplemental Material [33], Secs. S6 and Fig. S4). For example, the efficiency could be optimized for applications such as SPECT [54] or γ -ray burst detectors [55], where the emission rate is not a consideration. Medical applications could also exploit the larger number of photons per excitation to enable a lower x-ray dose or reduce the amount of radioactive material used. Alternatively, PhC designs can be optimized to increase the scintillation signal and thus reduce the treatment duration, or reduce the power consumption of x-ray machines by using lower x-ray flux or energy. Finally, the results shown here could reduce the amount of expensive scintillation material by replacing part of it with another material while maintaining (or increasing) the total scintillation emission.

The research is supported by the GIF Young Scientists' Program, by an ERC Starter Grant, and by the Israel Innovation Authority.

*kaminer@technion.ac.il

- [1] C. W. E. van Eijk, *Phys. Med. Biol.* **47**, R85 (2002).
- [2] P. Lecoq, A. Annenkov, A. Gektin, M. Korzhik, and C. Pedrini, in *Inorganic Scintillators for Detector Systems* (Springer-Verlag, Berlin, 2006).
- [3] R. A. Cecil, B. D. Anderson, and R. Madey, *Nucl. Instrum. Methods* **161**, 439 (1979).
- [4] G. Knoll, *Radiation Detection and Measurement*, 4th ed. (John Wiley, Hoboken, 2010).
- [5] F. A. Danevich, V. V. Kobychyev, R. V. Kobychyev, H. Kraus, V. B. Mikhailik, V. M. Mokina, and I. M. Solsky, *Nucl. Instrum. Methods Phys. Res., Sect. B* **336**, 26 (2014).
- [6] A. Benaglia, S. Gundacker, P. Lecoq, M. T. Lucchini, A. Para, K. Pauwels, and E. Auffray, *Nucl. Instrum. Methods Phys. Res., Sect. A* **830**, 30 (2016).
- [7] S. Gundacker, F. Acerbi, E. Auffray, A. Ferri, A. Gola, M. V. Nemallapudi, G. Paternoster, C. Piemonte, and P. Lecoq, *J. Instrum.* **11**, P08008 (2016).
- [8] S. Gundacker, R. M. Turtos, E. Auffray, M. Paganoni, and P. Lecoq, *Phys. Med. Biol.* **64**, 055012 (2019).
- [9] S. Derenzo, E. Bourret, S. Hanrahan, and G. Bizarri, *J. Appl. Phys.* **123**, 114501 (2018).
- [10] G. De Lorenzo, M. Chmeissani, D. Uzun, M. Kolstein, I. Ozsahin, E. Mikhaylova, P. Arce, M. Cañadas, G. Ariño, and Y. Calderón, *J. Instrum.* **8**, C01030 (2013).
- [11] Q. Li, J. Q. Grim, R. T. Williams, G. A. Bizarri, and W. W. Moses, *J. Appl. Phys.* **109**, 123716 (2011).
- [12] A. Hospodková, M. Nikl, O. Pacherová, J. Oswald, P. Brůža, D. Pánek, B. Foltynski, E. Hulicius, A. Beitlerová, and M. Heuken, *Nanotechnology* **25**, 455501 (2014).
- [13] R. M. Turtos, S. Gundacker, S. Omelkov, B. Mahler, A. H. Khan, J. Saaring, Z. Meng, A. Vasil'ev, C. Dujardin, M. Kirm, I. Moreels, E. Auffray, and P. Lecoq, *Npj 2D Mater. Appl.* **3**, 37 (2019).
- [14] M. Kronberger, E. Auffray, and P. Lecoq, *IEEE Trans. Nucl. Sci.* **55**, 1102 (2008).
- [15] A. Knapitsch and P. Lecoq, *Int. J. Mod. Phys. A* **29**, 1430070 (2014).
- [16] Z. Zhu, S. Wu, C. Xue, J. Zhao, L. Wang, Y. Wu, B. Liu, C. Cheng, M. Gu, H. Chen, and R. Tai, *Appl. Phys. Lett.* **106**, 241901 (2015).
- [17] A. Knapitsch, E. Auffray, C. W. Fabjan, J. L. Leclercq, P. Lecoq, X. Letartre, and C. Seassal, *Nucl. Instrum. Methods Phys. Res., Sect. A* **628**, 385 (2011).
- [18] Z. Zhu, B. Liu, C. Cheng, H. Zhang, S. Wu, M. Gu, H. Chen, L. Chen, J. Liu, and X. Ouyang, *Nucl. Instrum. Methods Phys. Res., Sect. A* **786**, 1 (2015).
- [19] M. Salomoni, R. Pots, E. Auffray, and P. Lecoq, *Crystals* **8**, 78 (2018).
- [20] A. Iltis, S. Zanettini, L. R. de Magalhaes, C. Tata, A. Soledade, M. Z. Hmissi, H. Khadiri, V. Gaté, and D. Turover, *J. Instrum.* **14**, P06036 (2019).
- [21] R. H. Pots, M. Salomoni, S. Gundacker, S. Zanettini, V. Gate, E. Usureau, D. Turover, P. Lecoq, and E. Auffray, *Nucl. Instrum. Methods Phys. Res., Sect. A* **940**, 254 (2019).
- [22] A. Lempicki, A. J. Wojtowicz, and E. Berman, *Nucl. Instrum. Methods Phys. Res., Sect. A* **333**, 304 (1993).
- [23] C. Greskovich and S. Duclos, *Annu. Rev. Mater. Sci.* **27**, 69 (1997).
- [24] M. Conti, *Phys. Med.* **25**, 1 (2009).
- [25] S. Gundacker, E. Auffray, K. Pauwels, and P. Lecoq, *Phys. Med. Biol.* **61**, 2802 (2016).
- [26] L. Hernández-Adame, F. Medellín-Rodríguez, A. Méndez-Blas, R. Vega-Acosta, and G. Palestino, in *Oxide-Based Mater. Devices IV* (International Society for Optics and Photonics, 2013), p. 86261P, <https://doi.org/10.1117/12.2004659>.
- [27] E. M. Purcell, *Phys. Rev.* **69**, 681 (1946).
- [28] D. Kleppner, *Phys. Rev. Lett.* **47**, 233 (1981).

- [29] E. Yablonovitch, *Phys. Rev. Lett.* **58**, 2059 (1987).
- [30] S. Enoch, G. Tayeb, P. Sabouroux, N. Gu erin, and P. Vincent, *Phys. Rev. Lett.* **89**, 213902 (2002).
- [31] S. Noda, M. Fujita, and T. Asano, *Nat. Photonics* **1**, 449 (2007).
- [32] L. Novotny and B. Hecht, *Principles of Nano-Optics* (Cambridge University Press, Cambridge, 2012).
- [33] See Supplemental Material at <http://link.aps.org/supplemental/10.1103/PhysRevLett.125.040801>, sections S.4 and S.5 for the derivation of the Dyadic Green's function, which includes Refs. [34,35].
- [34] W.C. Chew, *Waves and Fields in Inhomogeneous Media* (IEEE Press, New York, 1999).
- [35] J.A.E. Wasey and W.L. Barnes, *J. Mod. Opt.* **47**, 725 (2000).
- [36] S. Gundacker, Ph.D. thesis, Vienna University of Technology, 2014.
- [37] P. Lecoq, *Nucl. Instrum. Methods Phys. Res., Sect. A* **809**, 130 (2016).
- [38] R. F. Post and L. I. Schiff, *Phys. Rev.* **80**, 1113 (1950).
- [39] S. Surti, A. Kuhn, M. E. Werner, A. E. Perkins, J. Kolthammer, and J. S. Karp, *J. Nucl. Med.* **48**, 471 (2007), <http://jnm.snmjournals.org/content/48/3/471>.
- [40] Y. Ye, *Interior Point Algorithms: Theory and Analysis* (John Wiley & Sons, New York, 2011).
- [41] M. Yoshida, M. Nakagawa, H. Fujii, F. Kawaguchi, H. Yamada, Y. Ito, H. Takeuchi, T. Hayakawa, and Y. Tsukuda, *Jpn. J. Appl. Phys.* **27**, L1572 (1988).
- [42] J. D. Joannopoulos, S. G. Johnson, J. N. Winn, and R. D. Meade, *Photonic Crystals: Molding the Flow of Light* (Princeton University Press, Princeton, 2011).
- [43] M. J. Jurow, T. Morgenstern, C. Eisler, J. Kang, E. Penzo, M. Do, M. Engelmayr, W. T. Osowiecki, Y. Bekenstein, C. Tassone, L.-W. Wang, A. P. Alivisatos, W. Br tting, and Y. Liu, *Nano Lett.* **19**, 2489 (2019).
- [44] O. D. Miller, A. G. Polimeridis, M. T. Homer Reid, C. W. Hsu, B. G. DeLacy, J. D. Joannopoulos, M. Solja ic, and S. G. Johnson, *Opt. Express* **24**, 3329 (2016).
- [45] X. Lin, S. Easo, Y. Shen, H. Chen, B. Zhang, J. D. Joannopoulos, M. Solja ic, and I. Kaminer, *Nat. Phys.* **14**, 816 (2018).
- [46] C. Luo, M. Ibanescu, S. G. Johnson, and J. D. Joannopoulos, *Science* **299**, 368 (2003).
- [47] E. Norbeck, T. P. Dubbs, and L. G. Sobotka, *Nucl. Instrum. Methods Phys. Res., Sect. A* **262**, 546 (1987).
- [48] Y. Zorenko, V. Gorbenko, T. Voznyak, T. Martin, P.-A. Douissard, J. A. Mares, and M. Nikl, in *Non-Intrusive Inspection Technologies II* (International Society for Optics and Photonics, 2009), p. 731007, <https://doi.org/10.1117/12.818125>.
- [49] H. H. Sheinflux, Y. Lumer, G. Ankonina, A. Z. Genack, G. Bartal, and M. Segev, *Science* **356**, 953 (2017).
- [50] W. Kern and J. L. Vossen, *Thin Film Processes II* (Academic Press, San Diego, 2012).
- [51] Y. Shen, D. Ye, I. Celanovic, S. G. Johnson, J. D. Joannopoulos, and M. Solja ic, *Science* **343**, 1499 (2014).
- [52] W. Cheng, T. Gorishnyy, V. Krikorian, G. Fytai, and E. L. Thomas, *Macromolecules* **39**, 9614 (2006).
- [53] M. Nikl, *Meas. Sci. Technol.* **17**, R37 (2006).
- [54] M. T. Madsen, *J. Nucl. Med.* **48**, 661 (2007).
- [55] M. V. Medvedev and A. Loeb, *Astrophys. J.* **526**, 697 (1999).